Erschienen in: Advanced Functional Materials ; 29 (2019), 37. - 1902047
https://doi.org/10.1002/adfm.201902047

Symbiosis of Silica Biomorphs and Magnetite Mesocrystals

Julian Opel, Julian Brunner, Ramon Zimmermanns, Tristan Steegmans, Elena Sturm, Matthias Kellermeier, Helmut Cölfen,* and Juan-Manuel García-Ruiz**

Silica biomorphs are extraordinary inorganic superstructures formed via autocatalytic co-precipitation and bottom-up self-assembly of alkaline-earth carbonates and silica. However, they show no inherent functionality except for their striking textural motifs and curved morphologies. This work presents strategies to magnetize silica biomorphs, thus creating thermally stable ceramic microswimmers with unique elaborate shapes. This is achieved by growing super paramagnetic magnetite mesocrystals on and around the complex curved surfaces of biomorphs, while keeping their morphology and maintaining mesocrystal integrity. Selective mesocrystal formation on certain parts of the substrates is induced by chemical modification of the biomorph surface, increasing the loading of magnetite on the silica–carbonate structures and, in suitable cases, rendering them able to respond to external magnetic fields and move as microswimmer entities. In this way, the complex ultrastructure of silica biomorphs is successfully used as a template for functional ceramics. Furthermore, selective dissolution of the carbonate core from the biomorphs leads to hollow magnetic structures that could be filled with actives, thus serving as microcarriers with considerable loading capacity.

1. Introduction

Controlled movement on the microscale is a worthwhile goal in materials science. In principle, it necessitates a swimming unit and a responding unit or engine, which interacts with outer fields or converts fuel.[1] However, so far, it has been challenging to fabricate microswimmers with varying complex shapes within a single batch, which may enable interesting features such as self-propelling. Silica–carbonate "biomorphs" could be promising archetypes for the design of such swimming units, since they form spontaneously by self-assembly and grow into elaborate curved architectures on the multi-micrometer to millimeter scale.[2] Among the morphologies commonly displayed by these inorganic–inorganic hybrids, the most interesting shapes for swimming or carrying applications are the chiral filamentous forms, i.e., worm-like braids, helicoids, and twisted ribbons. All these peculiar structures can be obtained in a simple one-pot synthesis from aqueous media at ambient conditions. Indeed, biomorphs form on addition of alkaline-earth metal cations like barium, strontium, or calcium to alkaline, silica-rich solutions-, or gels, with subsequent diffusion of atmospheric CO_2 triggering the slow crystallization of carbonates under the influence of silicate species.[2a,3]

The formation of complex ultrastructures relies on an autocatalytic co-precipitation mechanism that produces uniform carbonate nanocrystals, which self-assemble on the mesoscale and become embedded in a matrix of amorphous silica.[2a] The rich structural variety of biomorphs is shown in **Figure 1**a–e (also compare with Figure S1a in the Supporting Information for an overview on typical structures obtained from a single batch) and can be explained based on differences in local growth velocities during the formation process, which can induce local curling and thus give rise to curved and twisted architectures.[3a,4] Once these structures are formed and self-assembly has ceased, secondary precipitation of silica (due to the lowered bulk pH) often leads to the deposition of a continuous skin of amorphous silica all over the structures.[5] Moreover, long reaction times can also cause secondary precipitation of (regular) carbonate crystals, which typically grow more or less selectively at the apex of the structures and their outer edges. In this stage, no coupled precipitation occurs and carbonate formation is preferred (note that both of these secondary processes will be used for functionalization below).

While many previous studies on silica biomorphs were focused on their morphogenesis and structural control[2b,3c,6] as well as relevance for primitive life detection,[3d] possible functional properties of biomorphs have hardly been explored until recently. The first successful surface functionalization of the as-obtained silica–carbonate hybrids was achieved using silane chemistry

J. Opel, J. Brunner, R. Zimmermanns, T. Steegmans, Dr. E. Sturm, Prof. H. Cölfen
Physical Chemistry
University of Konstanz
Universitätsstraße 10, D-78457 Konstanz, Germany
E-mail: helmut.coelfen@uni-konstanz.de
J. Opel, Prof. J.-M. García-Ruiz
Laboratorio de Estudios Cristalográficos
Instituto Andaluz de Ciencias de la Tierra (CSIC-UGR)
Avenida de las Palmeras N° 4, ES-18100 Armilla, Granada, Spain
E-mail: jmgruiz@ugr.es
Dr. M. Kellermeier
Material Physics
BASF SE
RAA/OS–B007, Carl-Bosch-Strasse 38, D-67056 Ludwigshafen, Germany
E-mail: matthias.kellermeier@basf.com

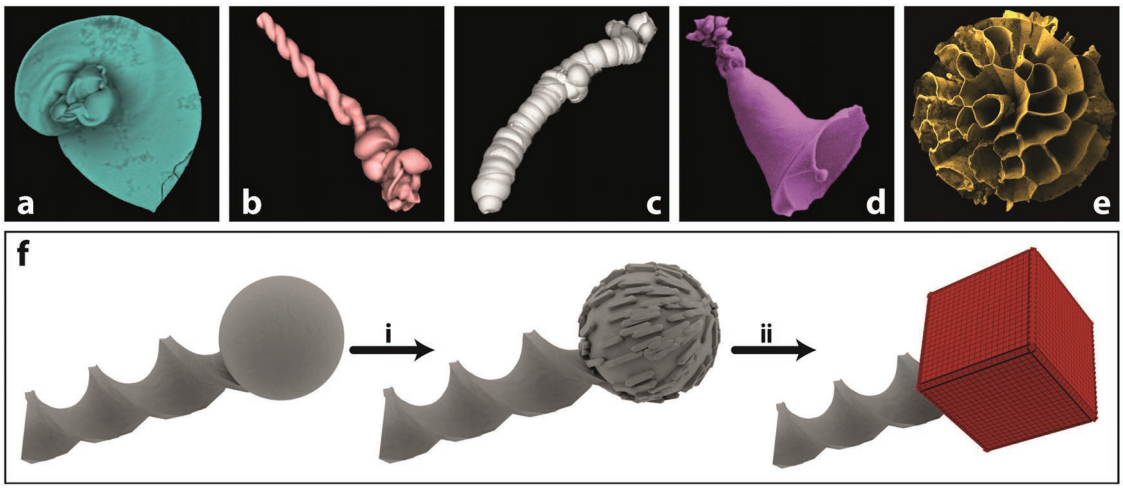

Figure 1. Morphological variety of silica biomorphs and the approach to magnetize them. a–e) Scanning electron microscopy images in false colors of a) a biomorphs' sheet, b) helix, c) worm-like braid, d) trumpet, and e) coral. f) Magnetization approach with magnetite mesocrystals. Methodological approach of the magnetization of silica biomorphs by heterogeneous nucleation of magnetite mesocrystals. In the first step, i) decoration of the globular end with witherite crystals is followed by ii) the selective mesocrystal formation.

in combination with nanoparticles or by controlled polymerization of organic matter around the inorganic template.[7] Later, the entire bulk composition of biomorphs was changed after growth by ion exchange and subsequent conversion to semiconducting perovskites.[8] In the present work, we have investigated the potential of biomorphs to serve as swimming units in microscale motors able to operate even at high temperature. Biomorph shapes which have a potential as a swimming unit are the helicoidally and the wormlike braids (cf. Figure 1b,c) and therefore this work focuses on this two types of morphologies.

To control the movement of silica biomorphs on the micrometer scale, they need to be equipped with a suitable engine or responding unit. One such engine could, in principle, be iron oxide catalysts, which would have to be immobilized on the biomorph surface, where they could then decompose hydrogen peroxide and generate gas bubbles that drive the motion of the microswimmers, as reported previously for other systems.[1a,9] However, since the size of biomorphs is typically in the range of at least tens of micrometers, they are likely too heavy to be propelled by this type of motor pretested. Instead, they require a stronger driving force—such as that provided by an external physical field. Here we have chosen to equip silica biomorphs with a magnetic responding unit that should allow them to navigate in an applied magnetic field. A suitable responding unit for magnetic biomorph microswimmers was obtained by particle-based crystallization, namely the assembly of super paramagnetic magnetite nanoparticles into "mesocrystals."[10] Mesocrystals are superstructures consisting of nanocrystals that share the preferred crystallographic orientation over long-range distances. Compared to bulk materials, nanocrystals often show outstanding size-dependent properties, but, in turn, they are difficult to handle as a material.[11] The assembly of nanocrystals into mesocrystals provides an important route to processability while maintaining the unique properties of nanocrystals during "scale-up" to micrometer-sized or even macroscopic structures. In the case of magnetite (Fe_3O_4), nanocrystals with sizes less than 30 nm show super paramagnetic behavior at room temperature.[12] This behavior allows them to affect mesocrystal formation using a magnetic field to create rather uncommon mesocrystals (in terms of morphology and structure) as compared to those formed without the influence of a magnetic field.[13] However, the super paramagnetic properties of the nanocrystals are preserved as reported for millimeter-sized mesocrystals, e.g., by Yin and co-workers and a further advantage is that the magnetic moments of the individual nanocrystals in the mesocrystal add up leading to excellent collective magnetization.[14] An advantage of super paramagnetic functionalized biomorphs is their preparation for further experiments compared to ferrimagnetic materials. Ferrimagnetic materials would permanently attract each other and simply agglomerate. A preparation of a single specimen would be rather difficult. For these reasons, magnetic mesocrystals seem to be a perfectly suited responding unit for microswimmers upon interaction with external magnetic fields. Uniting the concepts of silica biomorphs and magnetite mesocrystals, a variety of new self-assembled ultrastructures with interesting functional properties can be prepared via explicitly simple approaches, as summarized in Figure 1f. In this approach, a selective anchor point should be generated at its end with witherite crystals followed by the mesocrystal formation. The most promising symbiosis between barium carbonate (witherite) biomorphs and super paramagnetic mesocrystals—leading to high temperature stable (up to 420 °C), ceramic, responsive microarchitectures—is highlighted in this work.

2. Results and Discussion

Magnetite mesocrystals as responding unit for microswimmers were formed via gas diffusion of an antisolvent into an organic solvent–based dispersion of magnetite nanoparticles stabilized by oleic acid (see Figures S1b–d and S2a in the Supporting

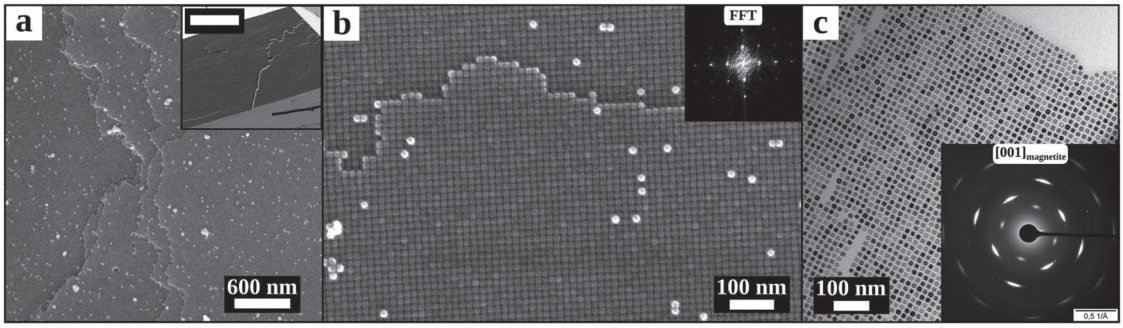

Figure 2. a,b) SEM images of mesocrystals at different magnifications to visualize the nanocrystal packing. Inset in panel (b): scale bars are 20 µm. The fast Fourier transformed (FFT) pattern shows the *p4mm* packing symmetry of the mesocrystal surface. c) Transmission electron microscopy (TEM) image of a mesocrystalline monolayer with its corresponding electron diffraction pattern. The indexed pattern is shown in Figure S2b (Supporting Information).

Information for details on the synthesis, a sketch of the setup used for the formation of mesocrystals and their imaging). The mesocrystals form on silicon wafers by a continuous and slow decrease of the colloidal stability of the nanoparticle dispersion, leading to well-defined superstructures as shown in **Figures 2** and **3**b,c, respectively.

Their morphology can be described as a tetragonal truncated pyramid exposing a *p4mm* projected symmetry on the basal (001) face, which shows *p4mm* plane group symmetry of nanoparticles packing (Figures 2a,b and 3b,c; Figure S1b–d, Supporting Information).[15] To act as a responding unit, these mesocrystals must crystallize on carbonate-rich surfaces as commonly displayed by biomorphs. This precondition was tested by replacing the usual silicon wafer as growth substrate with single crystals of aragonite (see Figure S2b in the Supporting Information) and calcite (see Figure S2c in the Supporting Information). Indeed, magnetite mesocrystals were found to grow on carbonate surfaces, with preferred occurrence on notches and roughness, indicating heterogeneous nucleation. Based on these observations, as-grown biomorphs were used directly and without any further chemical modification as microscopic substrates to create magnetic microswimmers in a straightforward procedure (Route III in Figure 3a). The result is shown in Figure 3g, demonstrating a successful combination of a biomorph worm and quite large magnetite mesocrystals, which have grown around the globular apex from which the worm has emerged. Here, selective attachment of the mesocrystals to the apex is ascribed to the presence of regular witherite crystals (i.e., bare carbonate surfaces without significant amounts of silica) on this part of the biomorph (as shown in Figure 3I and in Figure S3 in the Supporting Information), which have been generated by increasing the growth time from 8–10 h (bulk pH: 10.5) to 16–48 h (bulk pH: 8.5). At the lower bulk pH, the chemical coupling between carbonate and silicate speciation is no longer active; hence, the two components mineralize independently of one another (yielding regular carbonate crystals at the apex and a continuous silica skin over the rest of the aggregate). When the size of the magnetite mesocrystals is decreased (by adding less oleic acid stabilizer in the nanoparticle dispersion), the regular carbonate crystals covering the apex become visible and the selective growth of many small mesocrystals on these surfaces is clearly observed (see Figure 3e,i).

To further increase the mesocrystal loading, the surface of the biomorphs was modified in different ways, as summarized by the scheme in Figure 3a. This provides a toolbox allowing for the controlled deposition of mesocrystals at various positions of the biomorph, which would be impossible for nanocrystals only. For instance, treating the as-grown biomorphs with NaOH solution removes the outer silica layer (as proven by attenuated total reflection Fourier transformed infrared (ATR-FTIR) spectroscopy; cf. Figure 3d) and exposes their bare core, which consists mainly of co-aligned barium carbonate nanorods (Route I in Figure 3a). Such rough carbonate-rich surfaces should be an excellent substrate for the immobilization of magnetite nanocrystals enabling magnetite mesocrystal formation. Moreover, the obtained biomorphs without silica shell can be used to hydrophobize the surface via adsorption of a layer of oleic acid (Route II in Figure 3a; binding of oleic acid to the bare biomorph surface is confirmed by the two IR bands at 2852 and 2922 cm^{-1} in the black spectrum in Figure 3d). A hydrophobic surface should lead to enhanced interaction with the oleic acid stabilizer shell around the magnetite nanoparticles and thus to a denser coverage of the entire structure with the nanoparticles. Alternatively, biomorphs that still carry an outer silica skin can be hydrophobized by using alkyl triethoxysilanes (e.g., octadecyltriethoxysilane) (Route IV in Figure 3a).[7] Again, successful functionalization is shown by IR spectroscopy (Figure 3d).

Having obtained a collection of biomorphs exposing different surface chemistries (neat silica (hydrophilic), silane-modified silica (hydrophobic), neat carbonate (hydrophilic), and oleic acid–modified carbonate (hydrophobic)), we tested their ability to act as substrates for enhanced magnetite mesocrystal formation. Bare carbonate as well as hydrophobized surfaces (regardless of whether silanes or oleic acid is used) showed an increased, though less site-specific, adsorption of magnetite nanoparticles at various positions all over the biomorph architecture. The strong affinity of magnetite nanoparticles toward bare or hydrophobized surfaces is also supported by transmission electron microscopy (TEM) studies on crushed specimens. Figure 3f shows a single carbonate nanorod, which is decorated by numerous smaller magnetite particles. Analysis of several such carbonate rods suggests that they are covered with mono- or multilayers of magnetite nanocubes on most faces. Due to the strong affinity for magnetite to bind, bare carbonate and hydrophobic surfaces thus favor mesocrystal

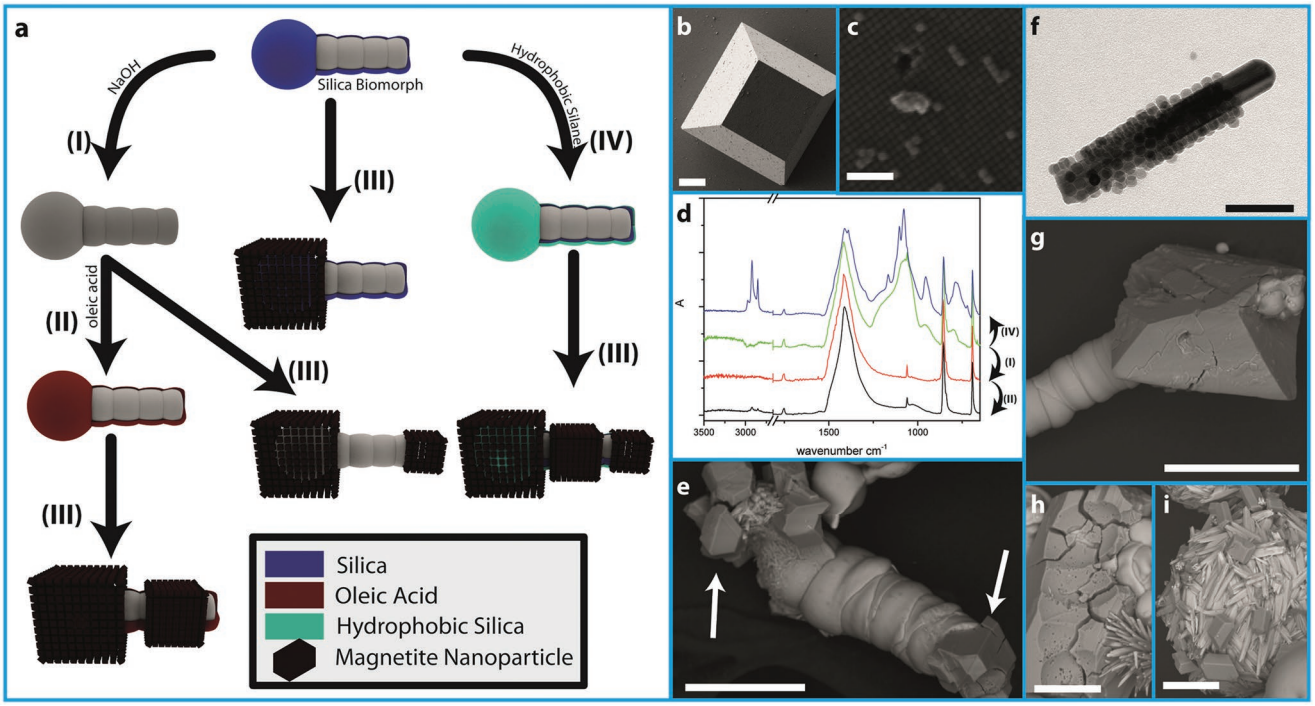

Figure 3. Functionalization of silica biomorphs with magnetite mesocrystals. a) Scheme illustrating the various pathways leading to different composites of magnetite mesocrystals and worm-like silica biomorphs. I) Dissolution of the outer silica shell of biomorphs with NaOH solution to obtain "naked" carbonate surfaces. II) Subsequent hydrophobization of the naked biomorph with oleic acid. III) Magnetite mesocrystal formation via "gas diffusion method" on top of the biomorph structure at different, potentially multiple positions. IV) Hydrophobization of the outer silica shell via post-treatment with alkyl triethoxysilanes. The indicated positions and amounts of the mesocrystals covering the biomorph worm are meant to illustrate the quality and selectivity of the functionalization. b,c) Scanning electron microscopy (SEM) images of magnetite mesocrystals grown from tetrahydrofuran (THF) solution upon destabilization via gas diffusion. d) ATR-FTIR spectra of biomorphs after modification according to pathways I, II, and IV in panel (a). e) SEM image showing the successful formation of magnetite mesocrystals (white arrows) around the apex and the tip of a worm-like biomorph that has been postfunctionalized with dodecyl triethoxysilane. f) TEM image of a carbonate nanocrystal obtained from the core of a biomorph, which was functionalized with oleic acid and subsequently became covered with magnetite nanocubes. g) SEM image of an unfunctionalized silica biomorph after mesocrystal formation. h) SEM image of a magnetite mesocrystal showing a negative imprint of a biomorph worm around which it originally grew. i) SEM image of the apex of a biomorph worm, which shows pronounced overgrowth with regular barium carbonate crystals (long rods), which themselves have been decorated by small magnetite mesocrystals (grown at reduced oleic acid concentration). Scale bars are b) 10 µm, c,f) 100 nm, e,g) 50 µm, and h,i) 25 µm, respectively.

formation on several different positions on one given biomorph architecture (cf. white arrows in Figure 3e), while on untreated biomorphs, rough areas like those carrying secondary witherite crystals (usually the globular apex, cf. Figure 3i) become preferentially overgrown by magnetite mesocrystals. The formation and growth of mesocrystals can also occur in between two or several neighboring biomorph structures, where the available (reduced) space is filled by the mesocrystals with no noticeable interference due to the confinement. One such example can be seen in Figure 3h, where a negative imprint of a biomorph worm is present on the mesocrystal (presumably the two domains were torn apart during isolation). This underlines the adaptability of the mesocrystals to existing template structures without abandoning the co-orientation of their nanoparticulate building units. In the light of the different presented functionalization methods as well as the broad intrinsic structural variability of silica biomorphs (including numerous other interesting morphologies beyond those addressed here, such as coral- or flower-like forms), it seems obvious that a large spectrum of magnetic microarchitectures can be designed using the concept introduced above. With respect to microswimmer applications, each of these forms may show different hydrodynamic behavior and thus can be selected from the morphological pool for a given purpose.

To test the response of the mesocrystal–biomorph composites to an external magnetic field, they were placed in a Petri dish that was mounted on a fixed platform under a light microscope (cf. **Figure 4**a–c). A permanent magnet (≈100 mT at the sample/290 mT at the magnet surface) was then fixed to the stage of the microscope underneath the sample, enabling an exact tracking of the position of the magnet. First, the swimming behavior in liquid media was studied by placing a magnetic microstructure (biomorph worm carrying two magnetite mesocrystals) on the surface of a highly viscous aqueous solution of (PEG, $M_W = 8000$ g mol^{-1}; 50 wt%; $\eta = 325.5$ mPa s), on which it floated randomly when no external field was applied. In the presence of the magnet, the superstructure can travel along predefined pathways through the solution (cf. Figure 4b; Movie S1 in the Supporting Information). Figure 4b′ shows a time-lapse sequence of images illustrating the linear movement of the responsive microarchitecture (see Movie S2 in the Supporting Information for the corresponding video)

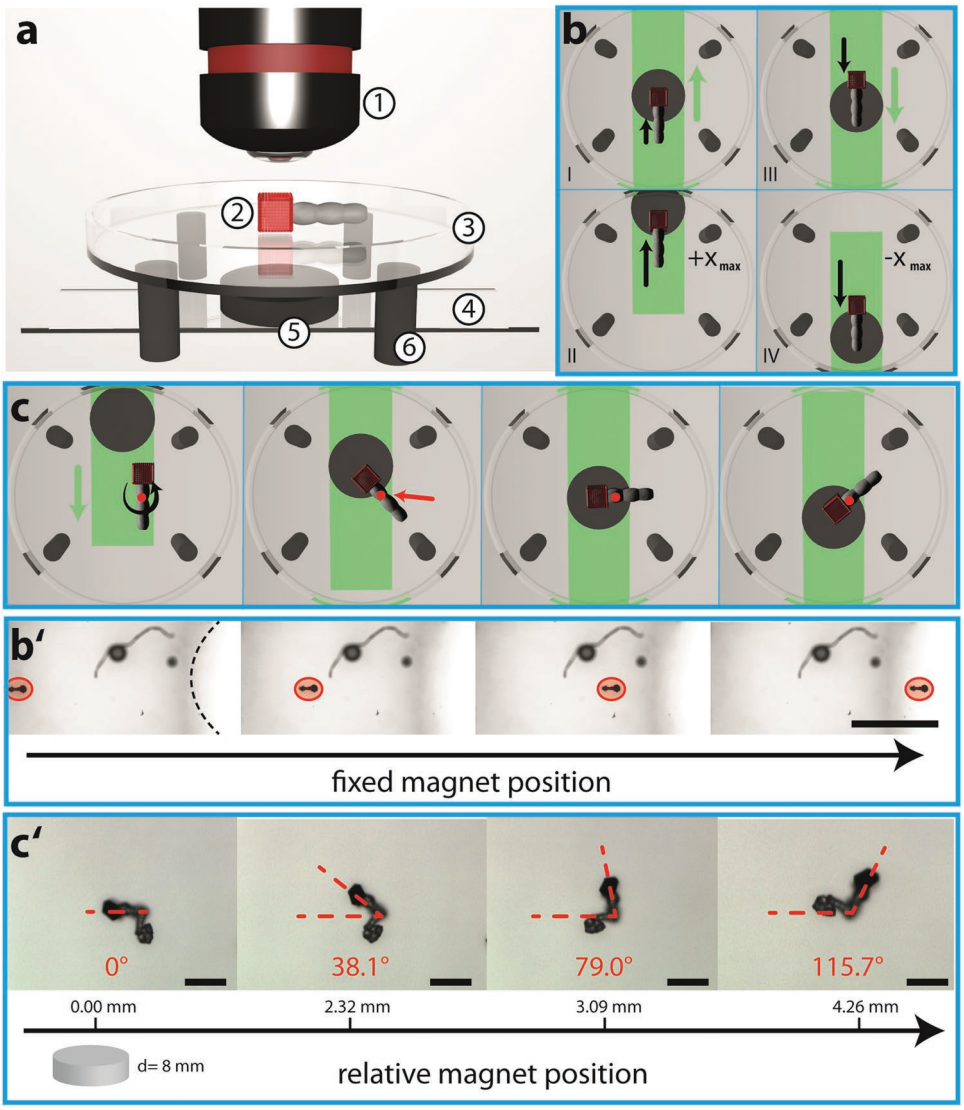

Figure 4. Biomorphs as responsive microarchitectures. a) Schematic illustration of the experimental setup used to move magnetized biomorphs in an external magnetic field—1: objective, 2: sample, 3: fixed Petri dish, 4: moving glass slide, 5: permanent magnet, and 6: holders for Petri dish. Moving the object holder will only displace the magnet (and not the sample), whose relative position is tracked at all times. b) Sketch of a linear displacement of a magnetized biomorph across a highly viscous aqueous polyethylene glycol (PEG) solution guided by a permanent magnet. Green and black arrows indicate the movement of the glass slide carrying the magnet below the Petri dish and the delayed response of the biomorph above, respectively. b′) Snapshots of an experiment according to the setup in panel (b), where the magnet is located at the right end of the field of view as indicated by the dashed black line, while the magnetized microstructure (highlighted in red) is moving toward it. Scale bars are 1 mm. c) Sketch of a rotating movement (indicated by the black arrow) of a dry magnetized biomorph in response to a linear displacement of the permanent magnet (green arrow). The red dot marks the position where the biomorph is fixed to the substrate (rotation axis), which in this case is not centered on the path travelled by the magnet. c′) Snapshots of an experiment according to the setup in panel (c). The biomorph–mesocrystal composite responds to the movement of the magnet (relative positions are given below the microscopic images) by rotation as indicated by the drawn angles. Scale bars are 100 µm.

induced by locating the magnet at a fixed position on the right side of the field of view (indicated by the black dashed line). The biomorph microswimmer moves directly toward the magnet through the viscous medium and can also be forced to travel forth and back following a continuous displacement of the magnet (as shown in Figure 4b and in Movie S3 in the Supporting Information). It is furthermore evident that response of the structure is somewhat delayed with respect to the displacement of the magnet, likely due to inertial effects caused by the high viscosity of the medium. In a second experiment, a biomorph worm carrying one magnetite mesocrystal at its apex (cf. Figure 3g) was put on a dry Petri dish, with its contact point (red dot in Figure 4c) slightly displaced relative to the center of the path travelled by the moving magnet. This induces a rotating movement when the magnet passes the structure, as illustrated schematically in Figure 4c and in Movie S4 (Supporting Information), and observed experimentally in Figure 4c′ and in Movie S5 (Supporting Information). Here, the self-assembled composite responds directly (due to the lower viscosity) to the displacement of the magnet

(relative magnet positions are indicated as pointing angles by the red lines in Figure 4c′, with 0° corresponding to the starting position). It should be noted that the biomorph–mesocrystal aggregate was not immobilized on the surface of the Petri dish, but nevertheless remained at a fixed position and only rotated. Furthermore, as can be seen in Movie S5 (Supporting Information), also single mesocrystals follow the movement of the magnet. They are a byproduct from the preparation procedure. This shows that the motion of the microarchitecture can be precisely controlled in the dry state if the applied forces are not too pronounced. All these observations clearly demonstrate that magnetite mesocrystals attached to silica biomorphs indeed work as responding units in an external magnetic field, enabling controlled movement on the micrometer scale.

Another very promising aspect about these materials is the possibility of transforming the magnetized architectures into hollow microcarriers, which can easily be achieved by removing the carbonate core with diluted acid, leaving behind a hollow silica "ghost" that still carries the mesocrystal responding unit. Such structures could serve as carriers for molecular cargo, which after filling with actives travel to predefined locations and release their cargo there (targeted microrelease and/or spatial reaction control in microenvironments). Movie S6 in the Supporting Information shows such a hollow ghost and its ability for controlled movement in an external magnetic field (note that this structure moves through a less viscous acetic acid solution and therefore the response to the moving magnet has no visible delay compared to the experiments in PEG solution). It could further be envisaged that the hollow silica framework is functionalized by silane chemistry to enable selective uptake and release.

At least, one should keep in mind that for a pure inorganic system with these responsive architectures, a high thermal stability is expected. To further investigate the thermal stability of mesocrystal–biomorph composites, the magnetite mesocrystals were annealed at different temperatures in the range between 350 and 500 °C, which is below the decomposition temperature of barium carbonate (Materials and Methods section in the Supporting Information). Within the tested temperature range, the specimens preserve the initial shape of the mesocrystals; however, at 350–420 °C the magnetite nanoparticles partially fuse together forming "mosaic" structures on the aggregate surfaces. At 500 °C, the phase transformation of magnetite to hematite is observed, and the faces of the specimens are overgrown by plate-like nanocrystals (Figure S4a, Supporting Information). Morphologically and compositionally the mesocrystal–biomorph composites should therefore be stable at least up to 420 °C. At even higher temperatures (1000 °C) the outer shape of the composite is still preserved (Figure S4b, Supporting Information), but new phases (including barium silicate, barium oxide, crystalline SiO_2 (tridymite), and hematite) have replaced the original materials which also goes along with a change of the magnetic responsivity.

3. Conclusion

In summary, our work highlights the successful symbiosis of two prominent examples for complex self-assembly in the field of crystallization: silica biomorphs and mesocrystals. Their combination leads to functional microscopic ultrastructures in straightforward processes at ambient conditions. Given the large variety of morphologies and structures accessible within one batch of biomorph synthesis (going far beyond the proof of concept established in this work), numerous types of responsive microtools can be generated in just a few processing steps. By targeted modification of the surfaces of silica biomorphs, the adsorption of super paramagnetite nanoparticles and their assembly into mesocrystals on the biomorph substrate can be controlled. This approach gives access to magnetic microarchitectures that can be applied as responsive tools ranging from microswimmers over microcarriers to micromanipulators. In the present work, it was demonstrated that external magnetic fields can be used to precisely control the movements of the architectures in a simplified setup. Since these structures are composed of purely inorganic material, they show high-temperature stability. Finally, the possibility of removing certain components selectively—e.g., carbonate by acid or silica by alkaline post-treatment, leaving a hollow silica ghost or an open porous carbonate network, respectively—offers further handles for enhanced functionality, such as the incorporation and/or transport of active compounds, which could eventually enable targeted release from the moving structure.

4. Experimental Section

Formation and Post-Treatment of Silica Biomorphs: Barium chloride dihydrate (>99%), sodium hydroxide (>98%), and sodium silicate solution (water glass with ≈10.6% Na_2O and ≈26.5% SiO_2, reagent grade) were purchased from Sigma Aldrich and used without further purification. All solutions were prepared using Milli-Q water with a conductivity of 18 µS cm^{-1}. The silicate solution for growth of biomorphs was obtained by diluting 1.39 g of sodium silicate solution in 349 mL of water. The pH was adjusted to 11.1 using 0.1 M sodium hydroxide solution. The resulting silica sol was then mixed in a 1:1 ratio with 0.01 M barium chloride solution in 6-well plates (Linbro). After 16 h exposure to the atmosphere, formed structures were recovered, washed several times with water and dried in air.

Hydrophobization of the as-obtained biomorphs with silanes was performed in an Eppendorf tube by dissolving 10 µL of the silane in 1.5 mL of a 4:1 EtOH:H_2O mixture. Then about 10 mg of biomorphs was added to the solution and incubated overnight. To dissolve the outer silica shell, 10 mg of biomorphs was incubated overnight in 1.5 mL of a 1 M sodium hydroxide solution. The silica-free biomorphs were then covered with a layer of oleic acid by overnight treatment with a sonicated mixture of 600 µL THF, 10 µL oleic acid, 10 µL 1 M NaOH, 2.5 mL cyclohexane, and 0.5 mL EtOH. All modified structures were cleaned by repeated washing with deionized water and centrifugation, followed by drying under reduced pressure.

Formation of Mesocrystal–Biomorph Composites: Iron oxide nanocrystals were prepared following a procedure described in the literature.[15a,16] Magnetite mesocrystals were obtained via destabilization of a nanocrystal dispersion in THF (5 mg mL^{-1} magnetite nanocrystals with 3 µL mL^{-1} oleic acid) in the presence of a piece of silicon wafer or powdered biomorphs in a glass vial. The glass vial was left in an outer surrounding reservoir, which contained EtOH:THF (1:1) as a destabilizing agent that slowly diffused into the nanoparticle dispersion via the gas phase. Complete destabilization of the nanocrystal dispersion and mesocrystal formation took about 1 week, as observed by a color change of the dispersion from black to colorless.

Thermal Annealing of Mesocrystals: In order to investigate the thermal stability, mesocrystals were annealed in an oven (Uni-Temp RTP-1200) under ultra high vacuum (UHV) conditions using a slow ramp rate. Primarily, the oven was heated up to 90 °C to evaporate the water out of the sample to avoid damage to the crystal upon expansion at high temperatures. After, the oven was heated to the desired temperature and kept at that temperature for 7 h before cooling down. Temperatures of 350, 380, 420, and 500 °C were investigated. The obtained samples were characterized by means of scanning electron microscopy (SEM) and X-ray diffraction (XRD).

Analytical Methods: The pH was controlled by a pH meter (Eutech pH 510). For polarized light microscopy (PLM), a Zeiss Imager M2m equipped with a $\lambda/4$ plate, EC Epiplan Neofluar objectives (5×, 10×, and 20×), a LD Epiplan 50× objective, and an Axiocam MRc 5 was used. SEM was performed with a Hitachi table-top SEM TM3000 at an acceleration voltage of 15 kV and a Zeiss Crossbeam at 5 kV. TEM studies were carried out on a Zeiss Libra 120 operated at an acceleration voltage of 120 kV. For measurement, the samples were mounted on carbon-coated 200 mesh Cu grids. ATR-FTIR measurements were performed on a Perkin-Elmer Spectrometer 100.

Acknowledgements

J.O. and J.B. contributed equally to this work. The authors thank SFB 1214 (Deutsche Forschungsgemeinschaft) project B1, the Particle Analysis Center (PAC) of the University of Konstanz, the Nanostructure Laboratory of the University of Konstanz, and the European Research Council ERC (Grant Agreement No. 340863).

Conflict of Interest

The authors declare no conflict of interest.

Keywords

barium carbonate, biomorph, magnetite, mesocrystal, microswimmer

[1] a) H. Wang, M. Pumera, *Chem. Rev.* **2015**, *115*, 8704; b) T. Li, J. Li, H. Zhang, X. Chang, W. Song, Y. Hu, G. Shao, E. Sandraz, G. Zhang, L. Li, J. Wang, *Small* **2016**, *12*, 6098; c) B. A. Grzybowski, H. A. Stone, G. M. Whitesides, *Nature* **2000**, *405*, 1033; d) J. Burdick, R. Laocharoensuk, P. M. Wheat, J. D. Posner, J. Wang, *J. Am. Chem. Soc.* **2008**, *130*, 8164.

[2] a) M. Kellermeier, H. Colfen, J. M. Garcia-Ruiz, *Eur. J. Inorg. Chem.* **2012**, *2012*, 5123; b) W. L. Noorduin, A. Grinthal, L. Mahadevan, J. Aizenberg, *Science* **2013**, *340*, 832; c) E. Nakouzi, O. Steinbock, *Sci. Adv.* **2016**, *2*, e1601144.

[3] a) J. M. García-Ruiz, E. Melero-García, S. T. Hyde, *Science* **2009**, *323*, 362; b) M. Kellermeier, E. Melero-Garcia, F. Glaab, J. Eiblmeier, L. Kienle, R. Rachel, W. Kunz, J. M. Garcia-Ruiz, *Chem. - Eur. J.* **2012**, *18*, 2272; c) J. Opel, M. Kellermeier, A. Sickinger, J. Morales, H. Cölfen, J.-M. García-Ruiz, *Minerals* **2018**, *8*, 75; d) J. M. Garcia-Ruiz, S. T. Hyde, A. M. Carnerup, A. G. Christy, M. J. Van Kranendonk, N. J. Welham, *Science* **2003**, *302*, 1194.

[4] M. Kellermeier, E. Melero-García, W. Kunz, J. M. García-Ruiz, *J. Colloid Interface Sci.* **2012**, *380*, 1.

[5] G. B. Alexander, W. Heston, R. K. Iler, *J. Phys. Chem.* **1954**, *58*, 453.

[6] a) E. Bittarello, F. Roberto Massaro, D. Aquilano, *J. Cryst. Growth* **2010**, *312*, 402; b) M. Kellermeier, F. Glaab, A. M. Carnerup, M. Drechsler, B. Gossler, S. T. Hyde, W. Kunz, *J. Cryst. Growth* **2009**, *311*, 2530; c) P. Knoll, E. Nakouzi, O. Steinbock, *J. Phys. Chem. C* **2017**, *121*, 26133.

[7] J. Opel, F. P. Wimmer, M. Kellermeier, H. Cölfen, *Nanoscale Horiz.* **2016**, *1*, 144.

[8] T. Holtus, L. Helmbrecht, H. C. Hendrikse, I. Baglai, S. Meuret, G. W. P. Adhyaksa, E. C. Garnett, W. L. Noorduin, *Nat. Chem.* **2018**, *10*, 740.

[9] J. Palacci, S. Sacanna, A. P. Steinberg, D. J. Pine, P. M. Chaikin, *Science* **2013**, *339*, 936.

[10] a) E. V. Sturm, H. Colfen, *Chem. Soc. Rev.* **2016**, *45*, 5821; b) H. Cölfen, M. Antonietti, *Angew. Chem., Int. Ed.* **2005**, *44*, 5576.

[11] a) H. Goesmann, C. Feldmann, *Angew. Chem., Int. Ed.* **2010**, *49*, 1362; b) D. V. Talapin, J.-S. Lee, M. V. Kovalenko, E. V. Shevchenko, *Chem. Rev.* **2010**, *110*, 389.

[12] a) J. Park, K. An, Y. Hwang, J. G. Park, H. J. Noh, J. Y. Kim, J. H. Park, N. M. Hwang, T. Hyeon, *Nat. Mater.* **2004**, *3*, 891; b) B. Faure, E. Wetterskog, K. Gunnarsson, E. Josten, R. P. Hermann, T. Bruckel, J. W. Andreasen, F. Meneau, M. Meyer, A. Lyubartsev, L. Bergstrom, G. Salazar-Alvarez, P. Svedlindh, *Nanoscale* **2013**, *5*, 953.

[13] J. J. Brunner, M. Krumova, H. Cölfen, E. V. Sturm, *Beilstein J. Nanotechnol.* **2019**, *10*, 894.

[14] J. Ge, Y. Hu, M. Biasini, W. P. Beyermann, Y. Yin, *Angew. Chem., Int. Ed.* **2007**, *46*, 4342.

[15] a) J. Brunner, I. A. Baburin, S. Sturm, K. Kvashnina, A. Rossberg, T. Pietsch, S. Andreev, E. Sturm, H. Cölfen, *Adv. Mater. Interfaces* **2017**, *4*, 1600431; b) L. Bergström, E. V. Sturm, G. Salazar-Alvarez, H. Cölfen, *Acc. Chem. Res.* **2015**, *48*, 1391; c) A. Ahniyaz, Y. Sakamoto, L. Bergström, *Proc. Natl. Acad. Sci. USA* **2007**, *104*, 17570.

[16] S. Disch, E. Wetterskog, R. P. Hermann, G. Salazar-Alvarez, P. Busch, T. Brückel, L. Bergström, S. Kamali, *Nano Lett.* **2011**, *11*, 1651.